Scientific Research Publishing

International Journal of Geosciences, 2022, 13, 438-463
https://www.scirp.org/journal/ijg
ISSN Online: 2156-8367
ISSN Print: 2156-8359

Upper Mantle Dynamic and Evolution beneath Lake Nyos Volcano (Cameroon Volcanic Line), Documented by Peridotite Xenoliths Enclosed in Alkali Basalts

Merlin Isidore Teitchou[1*], Joseph Legrand Tchop[1], Michel Grégoire[2], Eddy Ferdinand Mbossi[1], Pauline Wokwenmendam Nguet[1], Sahabo Aboubakar Abdoulaye[1], Ateba Bekoa[1]

[1]Institute for Geological and Mining Research, Buea, Cameroon
[2]Geosciences-Environnement Toulouse, UMR, Toulouse, France
Email: *teitchou.merlin@yahoo.fr

How to cite this paper: Teitchou, M.I., Tchop, J.L., Grégoire, M., Mbossi, E.F., Nguet, P.W., Abdoulaye, S.A. and Bekoa, A. (2022) Upper Mantle Dynamic and Evolution beneath Lake Nyos Volcano (Cameroon Volcanic Line), Documented by Peridotite Xenoliths Enclosed in Alkali Basalts. *International Journal of Geosciences*, **13**, 438-463.
https://doi.org/10.4236/ijg.2022.136024

Received: April 28, 2022
Accepted: June 20, 2022
Published: June 23, 2022

Abstract

Volcanic deposits from the lake Nyos contain ultramafic xenoliths: lherzolites, harzburgites and wehrlites, sometimes containing amphiboles and phlogopites. The lithospheric mantle beneath Nyos, as inferred from chemical diagrams, has experienced partial melting and variably cryptic and modal metasomatism of the two groups of samples that have been distinguished: Group 1 samples are characterized by spoon-shaped REE patterns, and Group 2 samples show light (L) REE-enriched patterns. Metasomatic events were associated with pervasive infiltration of volatile (Ti, CO_2, H_2O) or alkali-rich small melts fractions and fluids. Later on, hydrous phases, Ti-rich Cpx, CaO-rich Ol, Ti-rich Ol, Cr poor and low values of NiO and F_O (%) in wehrlite compared to other xenoliths, precipitated from alkali enrichments due to the percolation of the mantle by basaltic magmas. The metasomatic liquid which percolates the Nyos mantle column was a dense alkaline silicate rich in volatile, displaying low HFSE abundances in the metasomatic hydrous melts compared to the LILE. It is suggested that 1) cryptic metasomatism affected Group 1 samples, 2) the spinel-free wehrlite is a Group 2 sample corresponding to a cumulate of a similar melt and 3) amphibole may be a potassium-bearing mineral in addition to phlogopite at shallower levels of Nyos upper mantle. P-T estimated indicates that xenoliths were initially equilibrated in the garnet stability field, at depth of 85 Km, and then they were re-equilibrated in the spinel field owing to isobaric heating up to 1000˚C. Adiabatic decompressions occur from 85 to 50 Km materialized by sample NK14 showing transitional porphyroclastic to equigranular texture and displaying pyroxene-Cr

spinel symplectites, and from 50 to 30 Km corresponding to 8 - 18 Kbar, pressures in which most xenoliths were incorporated in the host lavas. Therefore, the presence of rising mantle plumes from 85 to 50 Km (sample NK14) and from 50 to 30 Km (all studied samples) is probably related to the evolution of heterogeneous translithospheric mantle diapirs beneath this section of the continental Cameroon Volcanic Line. Local diapirs here may be interpreted as rift-zone initiators.

Keywords

Nyos Xenoliths, Metasomatism, P-T Estimated, Mantle Diapirs, Rift-Zones

1. Introduction and Geological Setting

Since Paleocene time, magmatic activity occurred along a deep-seated fracture zone in West Africa: the Cameroon Volcanic Line (CVL, **Figure 1(A)**). CVL is an alignment of Tertiary to Recent oceanic and continental volcanoes and anorogenic plutons trending at averagely N30˚E and extending from the South Atlantic into Cameroon and Chad over a distance of 1600 Km [1] [2] [3] [4] [5]. The origin of this tectono-magmatic feature is still debated (e.g [2] [5]-[11]) and subject of controversy (Rift Zone? Hot Line implying DM + Focal Zone? Hot Spot? Translisthosperic Mantle Diapirs? etc.). The Nyos volcanic unit is part of the Oku Massif, one of the continental massifs of the CVL. In this unit, volcanism has been concentrated in distinct eruptive centres, the largest one being in the Lake Nyos area (**Figure 1(B)**). The Nyos volcanic rocks are almost alkali basalts [12]. Tholeiitic basalts have been also reported [13] [14]. Tholeiitic basalts seem older and derived by moderate partial melting than the alkali basalts that have been grouped into two successive episodes. The first manifestations have been termed the first episode [15] and are made up of large basaltic lava flow. The second episode (recent series) activity contrasts with the relatively quiet volcanism of the earliest volcanism activity in that it was highly explosive, giving rise to steep pyroclastic cones and maars. A recent series is a group of craters, tuff cones and mostly flows which, on the basis of their youthful morphology, are regarded as the products of some of the most recent activity in Oku massif. Lava flows, maar pyroclastic and cinder cones from the Lake Nyos Volcanic Unit (LNVU) enclose abundant ultramafic xenoliths of spinel lherzolites and harzburgites and a diverse suite of crustal rocks. Ultramafic xenoliths have not been found in the first episode. Ultramafic xenoliths comprise varying combinations of olivine, orthopyroxene, spinel, amphibole and phlogopite. In the present work, we document the petrography, mineralogy, thermobarometry and chemical data for bulk rocks and minerals in order to determine the nature, dynamic and geochemical evolution of the upper mantle underneath LNVU. The signification of Nyos mantle xenoliths properties in the context of CVL is debated.

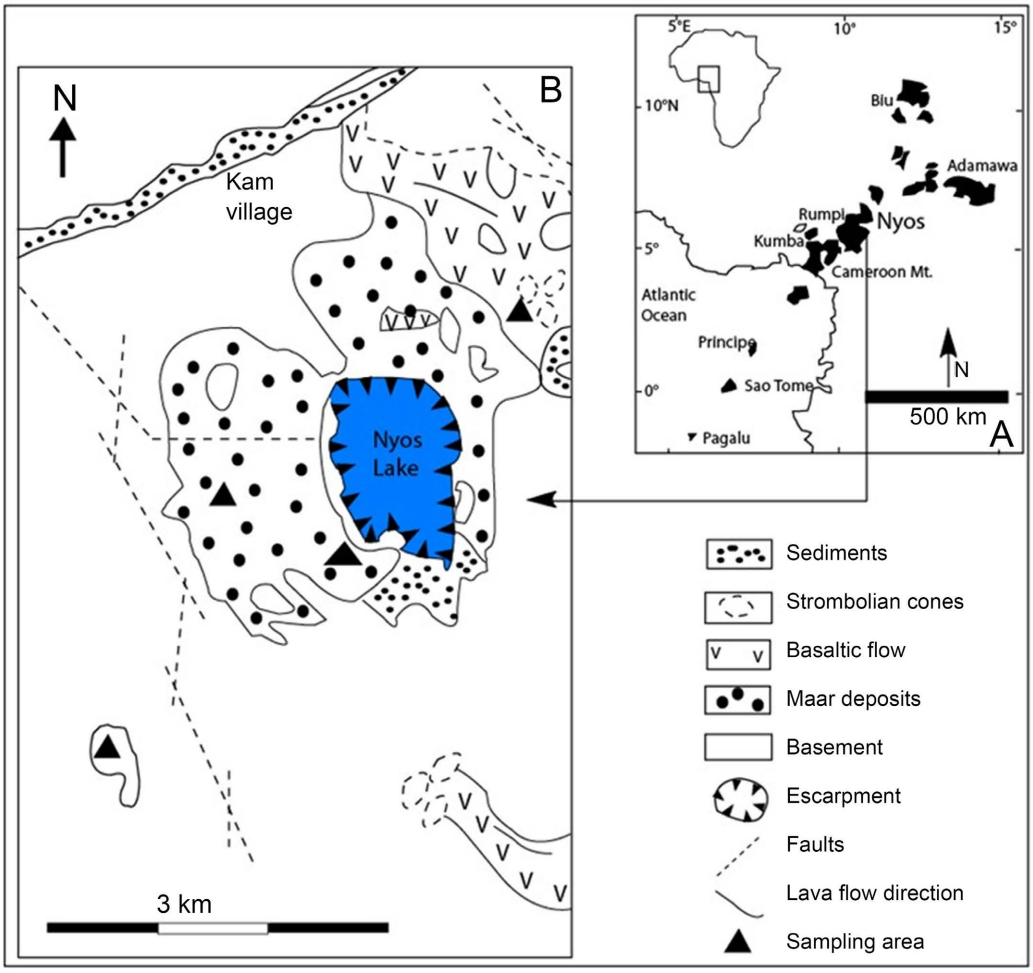

Figure 1. (A) Localization of the Cameroon volcanic line and (B) geological map of the Lake Nyos volcanic unit area.

2. Sample Description and Xenolith Petrography

More than twenty randomly selected ultramafic xenoliths were sampled from various areas of the LNVU. They are elliptical in shape and usually covered by thin crust basaltic lavas. Sizes range from few millimeters to more than ten centimeters.

Table 1 provides summary of the modal mineralogy of few and selected analyzed peridotites. It allows us to distinguish in Streckeisen diagram [16]: lherzolites, harzburgites with subsidiary wherlite (Figure 2). Websterites have been also reported [17] [18]. For the lherzolites, the original modal mineralogy is 54% - 75% olivine, 6% - 31% orthopyroxene, 5% - 19% clinopyroxene and 1% - 7% spinel. The average harzburgite has 76% - 85% olivine and 7% - 19% orthopyroxène, 1.5% - 3% clinpyroxene and 1% - 4% spinel. Amphibole is present in some samples but rarely exceeds 2% of the mode. Fluid inclusions and glass veinlets in some samples have been described by Touret *et al.* [19]. The spinel peridotites of the Nyos area are dominated by spinel lherzolites. Most samples have porphyoclastic texture (Figure 3(A), with olivine or orthopyroxene surround by smaller

Table 1. Modal compositions of the investigated Nyos mantle peridotites (in vol%).

Sample	Olivine	Orthopyroxene	Clinopyroxene	Spinel	Amphibole	Phlogopite
NK01	67	22	8	3	-	-
NK02	80	19	1	trace	1	-
NK04	73	20	2	3	-	2
NK05	71	16	9	4	-	-
NK07	67	17	11	5	-	-
NK08	63	-	37	-	-	-
NK09	60	19	8	3	-	-
NK10a	70	22	4	4	-	-
NK10b	73	21	3	3	-	-
NK11	69	22	8	1	-	-
NK13	63	25	10	2	-	-
NK14	66	18	15	trace	-	-
NK15	65	29	3	2	-	-

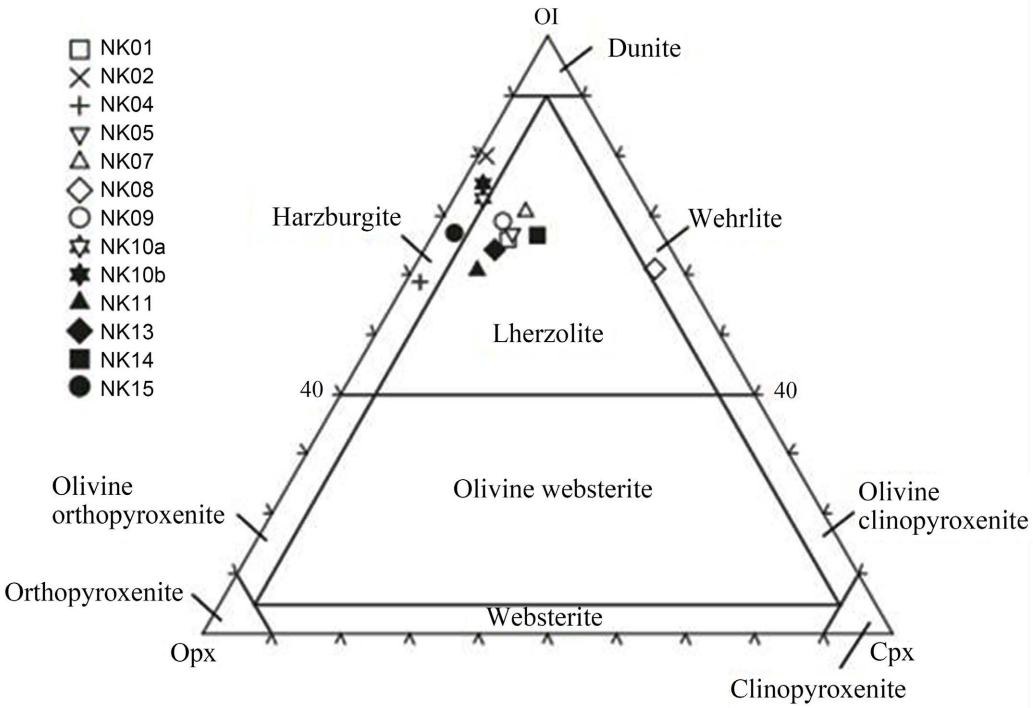

Figure 2. Modal composition of the studied Nyos xenoliths. Classification is after Streckeisen [16]. Ol—olivine; Opx—orthopyroxene; Cpx—clinopyroxene.

olivine neoblasts). Only few have protogranular texture (**Figure 3(B)**, coarse-grained olivine and orthopyroxene). Triple junctions are common and kink banding and undulatory extinction are present in some samples. Coarse grained orthopyroxenes contain abundant clinopyroxene exsolution lamellae, which are present at the center of the crystals.

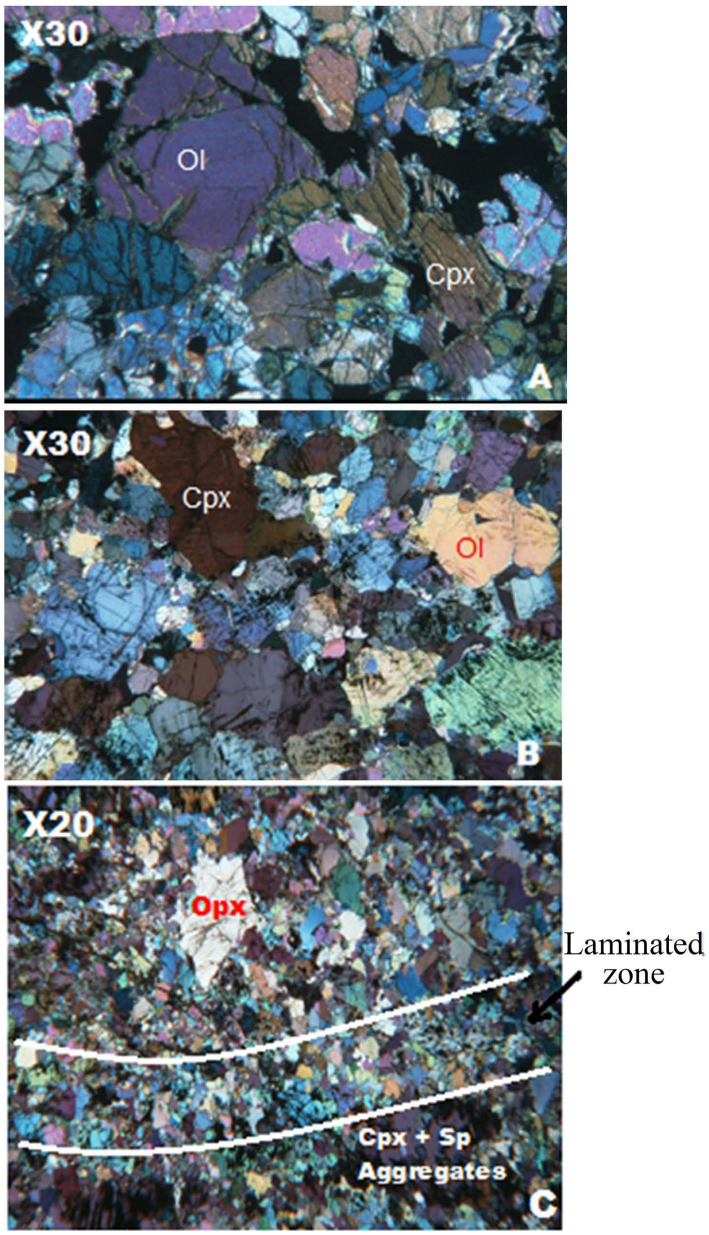

Figure 3. Microphotographs of (A) porphyroclastic texture; (B) protogranular texture; and (C) porphyroclastic to equigranular texture of sample NK14 showing a laminated zone.

All samples were studied petrographicaly and the five mineral phases in each xenolith described in the **Tables 2(A)-(E)** was analyzed on a CAMEBAX SX 50 electron microprobe using standard operating conditions. For more details concerning the analytical methods, see Teitchou *et al.* [10].

The spinel lherzolites show a wide variety of compositions, ranging from rather fertile or enriched lherzolites (Group 2) to depleted lherzolites (Group 1) with 9% to 30% orthopyroxene and 19% to 5% clinopyroxene. The fact that spinels have low values of Cr# and medium to high values of Mg# excluded a magmatic origin of these minerals.

Table 2. (A) Representative microprobe analyses of cores of olivines; (B) Representative microprobe analyses of cores of orthopyroxenes; (C) Representative microprobe analyses of cores of clinopyroxene; (D) Representative microprobe analyses of cores of spinel; (E) Representative microprobe analyses of cores of amphibole.

(A)

	Group 1 Lherzolite	Group1 Lherzolite	Group 1 Lherzolite	Group 1 Lherzolite	Group 1 Harzburgite	Group 1 Lherzolite	Group 1 Harzburgite	Group 1 harzburgite	Group 2 harzburgite	Group 2 Lherzolite	Group 2 Wehrlite
Olivine	NK01	NK05	NK07	NK09	NK10	NK11	NK15	NK02	NK04	NK14	NK08
SiO_2 (wt%)	40.90	41.10	41.71	40.82	41.03	41.44	41.64	41.29	40.51	40.87	38.95
TiO_2	0.03	-	-	-	0.01	-	-	-	0.03	-	0.01
Al_2O_3	-	-	-	-	-	-	-	-	-	-	-
Cr_2O_3	0.04	0.01	0.01	0.03	0.01	0.02		0.02		0.02	0.03
FeOtotal	10.10	9.90	9.95	9.66	9.66	9.84	9.95	9.58	12.20	12.57	19.86
MnO	0.13	0.15	0.13	0.1	0.13	0.12	0.19	0.15	0.16	0.19	0.30
MgO	49.59	50.08	49.49	49.87	49.94	49.19	49.48	49.81	47.62	47.38	41.81
CaO	0.09	0.09	0.12	0.06	0.11	0.11	0.06	0.09	0.07	0.09	0.26
NiO	0.36	0.37	0.39	0.32	0.29	0.25	0.38	0.32	0.45	0.17	0.04
Total	101.23	101.66	101.79	100.85	101.17	100.98	101.71	101.26	101.04	101.29	101.25
MgO#	89.75	90.02	89.86	90.20	90.21	89.91	89.86	90.26	87.43	87.04	78.95

(B)

Orthopyroxene	NK01	NK05	NK07	NK09	NK10	NK11	NK15	NK02	NK04	NK14
SiO_2 (wt%)	55.43	55.36	57.10	56.48	55.70	56.06	56.62	56.76	55.93	54.56
TiO_2	0.06	0.04	0.01	0.05	0.04	-	0.06	0.01	0.04	0.13
Al_2O_3	4.34	4.46	3.74	3.65	3.75	3.66	3.79	3.23	2.43	-
Cr_2O_3	0.40	0.46	0.29	0.33	0.39	0.35	0.40	0.46	0.40	0.47
FeOtotal	6.53	6.44	6.59	6.58	6.22	6.51	6.39	5.99	7.81	7.83
MnO	0.13	0.13	0.12	0.13	0.17	0.10	0.16	0.11	0.12	0.21
MgO	33.44	33.34	33.76	33.61	34.02	33.33	33.63	33.8	32.95	32.44
CaO	0.76	1.32	0.76	0.60	0.57	0.74	0.63	0.77	0.85	0.81
Na_2O	-	0.01	-	-	-	-	-	-	-	-
K_2O	-	0.01	-	0.01	0.01	-	-	-	-	-
Total	101.19	101.74	102.37	101.45	100.98	100.76	101.66	101.13	100.63	100.51
Mg#	90.13	90.21	90.13	90.11	90.70	90.12	90.36	90.96	88.27	88.08

(C)

Clinopyroxene	NK01	NK05	NK07	NK09	NK10	NK11	NK15	NK02	NK04	NK14	NK08
SiO_2 (wt%)	52.19	52.43	52.47	52.26	51.74	52.45	53.45	52.46	52.90	52.13	47.68
TiO_2	0.25	0.20	0.30	0.27	0.41	0.32	0.31	0.25	0.22	0.50	1.77
Al_2O_3	5.34	5.37	5.67	5.13	5.98	5.70	5.13	4.40	3.22	4.54	8.10
Cr_2O_3	0.72	0.66	0.79	0.63	0.85	0.81	0.78	1.26	0.71	1.10	0.14
FeOtotal	3.07	3.10	3.17	2.96	2.84	3.08	2.78	3.07	3.36	4.05	6.67
MnO	0.10	0.07	0.10	0.093	0.08	0.043	0.09	0.10	0.07	0.13	0.16

Continued

MgO	16.11	16.28	15.75	16.05	15.12	15.68	15.84	16.19	16.61	15.90	13.35
CaO	22.05	21.69	21.65	21.94	21.56	21.53	21.67	21.70	23.15	21.69	21.50
Na_2O	0.88	1.09	1.02	1.07	-	1.11	1.24	0.81	0.43	0.90	0.63
K_2O	-	0.01	-	-	-	0.01	0.01	0.02	0.04	0.01	-
Total	100.72	100.89	100.92	100.62	98.58	100.73	101.31	100.24	100.72	100.94	99.98
Mg#	90.33	90.35	89.86	92.97	90.47	90.07	91.03	90.38	89.79	87.50	78.10

(D)

Spinel	NK01	NK05	NK07	NK09	NK10	NK11	NK15	NK02	NK04	NK14
SiO_2 (wt%)	0.05	0.03	0.04	0.03	0.02	0.04	0.03	0.05	0.06	0.07
TiO_2	0.03	0.03	0.06	0.03	0.03	0.04	0.06	0.04	0.36	0.53
Al_2O_3	55.08	55.67	54.91	55.48	55.32	55.21	54.82	38.46	35.63	31.79
Cr_2O_3	11.64	11.3	11.49	11.47	11.94	11.32	12.43	27.99	27.15	29.85
Fe_2O_3	3.78	3.98	3.99	3.08	3.01	3.42	2.25	6.49	6.54	8.94
FeO	9.76	9.20	9.32	9.47	9.39	9.36	9.37	9.38	15.11	14.11
MnO	0.12	0.11	0.11	0.10	0.07	0.11	0.11	0.16	0.16	0.18
MgO	20.13	20.63	20.40	20.28	20.39	20.26	20.09	17.52	14.54	15.20
ZnO	0.08	-	-	-	-	-	0.06	-	0.24	-
NiO	0.36	0.43	0.34	0.33	0.28	0.41	0.37	0.18	0.27	0.26
Total	101.03	101.39	100.67	100.26	100.44	100.16	99.57	100.26	100.06	100.91
Mg#	73.16	74.20	73.80	74.70	75.07	74.38	75.86	67.23	55.25	55.01
Cr#	12.42	11.99	12.31	12.18	12.65	12.09	13.21	32.81	33.82	38.65

(E)

Amphibole	NK02	Phlogopite	NK04
SiO_2 (wt%)	43.74	SiO_2 (wt%)	38.62
TiO_2	1.40	TiO_2	2.92
Al_2O_3	13.56	Al_2O_3	15.84
Cr_2O_3	2.10	Cr_2O_3	0.92
FeOtotal	4.07	FeOtotal	4.59
		ZnO	0.03
MnO	0.07	MnO	0.05
MgO	17.43	MgO	22.20
CaO	11.07	CaO	0.01
Na_2O	3.09	Na_2O	0.54
K_2O	1.15	K_2O	9.45
		BaO	0.29
NiO	0.08	NiO	0.23
Total	97.75	Total	95.69
Mg#	88.42	Mg#	89.61

Olivine commonly forms porphyroclasts, which form the principal mineral within the peridotites. The porphyroclasts can be up to 5 mm long and 4 mm wide, although smaller grains less than 2 mm are also common. Olivine also forms small neoblasts (0.1 - 0.05 mm) which are principally found at the grain boundaries of both olivine and orthopyroxene porphyroclasts and have lobate grain boundaries. Olivine compositions vary little in the same type of xenolith. The olivines of the spinel lherzolites are remarkably similar averaging $F0_{88}$ in the least depleted (lherzolites Group 1). The olivine of the spinel harzburgites are more forsteritic, with the averaging composition $F0_{91}$. The NiO content of olivines range from 0.10 to 0.3 wt% and show no correlation with Fo content. The CaO content of all olivines are less than 0.1 wt%. The olivines of spinel wherlite are less forsteritic with Fo_{78}.

Orthopyroxene is generally found as porphyroclasts of varying size ranging from 1 to 6 mm long and 4 mm wide and as neoblasts. Exsolution lamellae of clinopyroxene are common within orthopyroxene porphyroclasts. Orthopyroxene grains show obvious signs of both ductile and brittle deformation. Compositionally, the orthopyroxene are magnesian with low contents of CaO (0.2 wt%) in clinopyroxene- poor peridotites to an average of 0.5% in clinopyroxene-rich peridotite and Al_2O_3 (usually 1 - 2 wt% and rarely exceeding 3 wt%). The average compositions of the orthopyroxenes in the various xenoliths groups are as follows: spinel lherzolites $Wo_2En_{86}Fs_{12}$. Orthopyroxenes in spinel harzburgite are higher in MgO and Cr_2O_3, lower in Al_2O_3 and TiO_2 than in the spinel lherzolites.

Clinopyroxene makes up a very small part of the mode of peridotites. The average compositions of the clinopyroxenes in the two groups are as follows: spinel harzburgite- $Wo_{42}En_{51}Fs_7$; spinel lherzolites – $Wo_{40}En_{54}Fs_6$. Clinopyroxenes have a fairly restricted range in Mg-number [atomic $Mg/(Mg + Fe^{2+})$] of 0.88 - 0.90 and range in Al_2O_3 and Cr_2O_3 content from 4.5-6.2 wt% respectively. K_20 contents are less than 0.10 wt%.

Spinel is a ubiquitous phase in the Nyos peridotites with a modal abundance of 2% - 7% in harzburgite and up to 9% in some of the lherzolite samples. The spinels exhibit a restricted variation in Cr number or Cr# [atomic Cr/(Cr + Al)] from just over 0.064 to nearly 0.239. Spinels in spinel fertile lherzolite exhibit almost the full range of Cr# where as those from depleted lherzolites show more restricted range of 0.064 - 0.150. The Fe_2O_3 content of spinels in lherzolites rarely exceeds 3 wt%, whereas spinels in harzburgites have Fe_2O_3 content between 3 and 4 wt%. Some minerals show sign of alteration processes.

Amphibole is found in some peridotites but rarely exceeds 2% of the mode. They are magnesium number rich with Mg-number between 0.928 and 0.964, and have appreciable TiO_2 (>3 wt%) and K_2O (>2 wt%) and low contents of chromium and aluminum (1.3 wt% Cr_2O_3 and <15 wt% Al_2O_3). Compositionally ($Ca/Na > 1$; $Ca + Na > 1.34$, and $Na < 0.67$; $Al^{IV} > Fe^{3+}$) they are pargasitic amphibole [20]. This pargasitic amphibole shows chemical similarities with amphibole peridotites of the CVL [4].

3. Geochemical Characteristics

LA-ICPMS data of clinopyroxenes, amphiboles and phylogopites are given in Table 3(A) & Table 3(B) Trace elements in same samples are available using ICP-MS solution. Table 4 displays the results of bulk rock major-element by XRF analysis and trace element ICPMS solution data obtained only on five samples at the University of Saint Etienne (France).

Table 3. (A) Representative clinopyroxene trace-element analyses (LA-ICP-MS) of Nyos peridotites (values in ppm); (B) Representative amphibole and phlogopite trace-element analyses of Nyos peridotites (values in ppm).

(A)

Sample	Group 1 Harzburgite	Group 1 Harzburgite	Group 1 Harzburgite	Group 1 Lherzolite	Group 1 Lherzolite	Group 1 Lherzolite	Group 1 Lherzolite	Group 2 Lherzolite	Group 2 Larzburgite	Group 2 Wehrlite
	NK02	NK10	NK15	NK01	NK05	NK09	NK11	NK14	NK04	NK08
Sc	66.35	61.48	73.91	61.72	60.97	57.78	58.04	55.11	55.56	69.58
Ti	461.98	1608.62	2006.4	1702.56	1643.34	1799.66	1847.82	3563.77	1182.25	10,465.00
V	151.82	229.97	254.97	230.11	218.95	226.07	228.39	248.55	134.55	295.46
Ni	228.38	289.01	256.10	276.37	249.36	272.56	271.42	247.02	247.58	101.95
Rb	0.77	2.94	0.77	2.88	3.27	2.39	3.75	3.16	1.18	1.39
Sr	147.23	18.53	6.23	20.03	20.18	12.17	11.86	125.28	102.61	98.73
Y	13.40	15.40	16.08	16.21	16.31	14.72	18.32	15.11	10.11	10.29
Zr	19.32	12.12	7.41	12.17	12.92	9.32	13.56	56.22	108.46	78.05
Nb	0.37	0.21	0.08	0.25	0.20	0.13	0.21	0.59	0.17	0.94
Ba	7.37	26.40	2.82	26.53	33.26	20.66	34.77	29.32	9.13	5.79
La	13.26	1.67	0.09	1.70	1.44	0.26	0.51	9.43	8.04	6.15
Ce	22.05	2.37	0.29	2.47	1.83	0.68	0.96	23.18	30.15	17.46
Pr	2.01	0.25	0.09	0.24	0.20	0.16	0.12	3.28	5.53	2.93
Nd	6.90	1.48	1.07	1.31	1.04	1.37	1.18	15.12	28.22	15.80
Sm	1.51	0.82	0.71	0.72	0.66	0.81	0.78	4.34	6.94	4.99
Eu	0.51	0.40	0.41	0.38	0.35	0.40	0.43	1.42	1.71	1.68
Gd	1.71	1.55	1.69	1.63	1.51	1.55	1.85	3.81	4.27	4.75
Dy	2.13	2.20	2.42	2.29	2.25	2.13	2.50	3.51	3.77	4.28
Ho	0.47	0.52	0.58	0.55	0.55	0.50	0.58	0.70	0.62	0.75
Er	1.35	1.59	1.65	1.65	1.64	1.49	1.66	1.78	1.46	1.63
Yb	1.40	1.58	1.58	1.58	1.57	1.50	1.59	1.59	1.21	1.28
Lu	0.20	0.22	0.22	0.22	0.21	0.21	0.23	0.22	0.15	0.14
Hf	0.45	0.50	0.47	0.51	0.54	0.49	0.65	1.31	2.93	3.59
Ta	0.01	0.02		0.03	0.03	0.01	0.02	0.07	0.03	0.14
Th	0.34	0.26	0.03	0.34	0.37	0.08	0.22	0.81	0.38	0.21
U	0.23	0.16	0.03	0.16	0.22	0.10	0.17	0.27	0.07	0.08

(B)

	Group 1 Amphibole Amp harzburgite NK02	Group 2 Phlogopite Phl harzburgite NK04
Sc	43.78	8.79
Ti	2132.40	17412.84
V	207.7	212.70
Ni	295.63	1333.66
Rb	3.03	360.97
Sr	136.21	137.34
Y	13.50	0.23
Zr	32.43	17.94
Nb	9.06	8.75
Ba	31.24	2973.66
La	12.08	-
Ce	20.30	0.32
Pr	2.09	-
Nd	7.18	0.21
Sm	1.49	0.45
Eu	0.52	0.12
Gd	1.71	0.10
Dy	2.06	-
Ho	0.45	-
Er	1.35	0.03
Yb	1.40	0.05
Lu	0.21	-
Hf	0.81	0.54
Ta	0.41	0.58
Th	0.45	0.05
U	0.16	0.05

Table 4. Bulk Rock major-element data (X-Ray Fluorescence) and trace-element data (ICP-MS solution) of Nyos peridotites.

	Group 1 Lherzolite	Group 1 Lherzolite	Group 1 Lherzolite	Group 1 Harzburgite	Group 2 Phl-Harzburgite
	NK01	NK05	NK11	NK10	NK04
SiO_2	43.59	43.74	45.4	44.1	45.94
TiO_2	0.07	0.07	0.08	0.08	0.11
Al_2O_3	2.7	2.77	3.09	2.89	1.68

Continued

Fe_2O_3	8.93	8.5	8.38	9.12	10.32
MnO	0.14	0.14	0.14	0.15	0.16
MgO	40.91	41.29	40.31	41.16	40.18
CaO	2.63	2.64	2.39	2.72	0.94
Na_2O	-	-	-	-	-
K_2O	-	-	-	-	0.03
P_2O_5	0.02	0.02	0.01	0.02	0.03
Total	99	99.17	99.79	100.23	99.39
Mg#	89.09	89.64	89.56	88.95	87.41
Sc	14.35	15.02	17.00	18.84	11.30
Ti	431.64	413.66	485.60	455.62	641.47
V	64.80	66.60	68.80	70.70	37.90
Cr	2844.20	2652.80	2910.00	2972.50	2934.20
Co	110.30	110.20	102.40	109.70	123.00
Ni	2145.60	2238.90	2040.70	2181.70	1983.20
Cu	15.60	5.9	2.70	16.60	24.20
Zn	53.20	46.00	48.90	63.30	64.50
Ga	1.32	1.61	1.80	1.88	1.92
Rb	0.06	0.04	0.032	0.07	3.29
Sr	2.98	1.32	0.50	3.14	4.34
Zr	1.18	0.64	0.84	1.28	6.55
Nb	0.15				0.19
Ba	2.96	1.09	1.37	3.76	31.37
La	0.45	0.23	0.20	0.60	0.59
Ce	0.59	0.32	0.31	0.87	1.50
Pr	0.07	0.04	0.04	0.11	0.24
Nd	0.35	0.24	0.22	0.49	1.13
Sm	0.11	0.10	0.09	0.16	0.28
Eu	0.05	0.05	0.04	0.07	0.08
Gd	0.23	0.21	0.23	0.26	0.20
Tb	0.04	0.04	0.05	0.05	0.03
Dy	0.32	0.31	0.37	0.40	0.19
Ho	0.08	0.08	0.09	0.09	0.04
Er	0.24	0.23	0.28	0.31	0.11
Tm	0.04	0.03	0.04	0.04	0.02
Yb	0.25	0.25	0.30	0.32	0.12
Lu	0.04	0.04	0.05	0.05	0.02
Th	0.04	0.04		0.04	0.04
U	0.01	0.02	0.01	0.02	0.02

The data have been plotted in MgO vs major and some trace elements. MgO acts here as an index of depletion [21], increasing in value as the rock becomes more depleted. Variations of major oxides as a function of MgO are plotted in Figure 4. The variation observed are similar to the general trend obtained in spinel peridotites from other localities around the world (e.g. Massif Central and Ronda [22] [23]). As a whole, a negative correlation exists between SiO_2, Al_2O_3, Na_2O, TiO_2 and CaO that may correspond to a series of residues from which an increasing amount of basaltic melt component had been removed [24] [25]. Following the conventional view, these trends are interpreted as resulting from variable degrees of partial melting of the upper mantle. As shown in Figure 4, the group I lherzolites have high Al_2O_3 and low CaO contents, reflecting a low degree of depletion of basaltic components. These fertile or enriched samples have also high modal propositions of clinopyroxenes. In contrast, the lherzolites group II and harzburgites, with lower Al_2O_3 and CaO contents are more depleted. Some of the lherzolites group I have compositions (MG > 88) commonly accepted as primitive mantle [24] [26] [27]. These samples display K_2O, Na_2O, and P_2O_5 contents close to or below the detection limits, while their TiO_2 content is very low (<0.2 wt%). Elements that show good correlation with MgO within the peridotites from Nyos area are Y, Yb (representing HREE) V, Co and Ni (Figure 5). Co and Ni, which are compatible during melting, have positive trends. The degree of melting is estimated of around 5% (see Figure 6, for further explanations, normalizing values are from Johnson *et al.* [28]) in low enriched

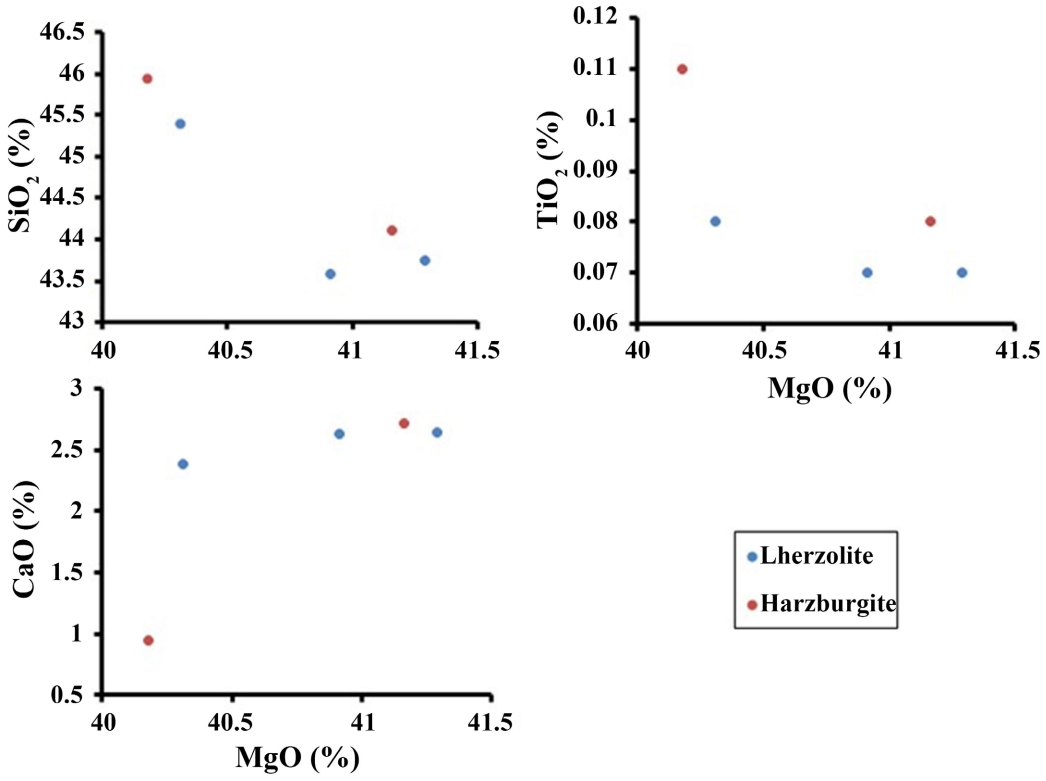

Figure 4. Variations of major oxides (SiO_2, Al_2O_3, Na_2O, TiO_2 and CaO) as a function of MgO.

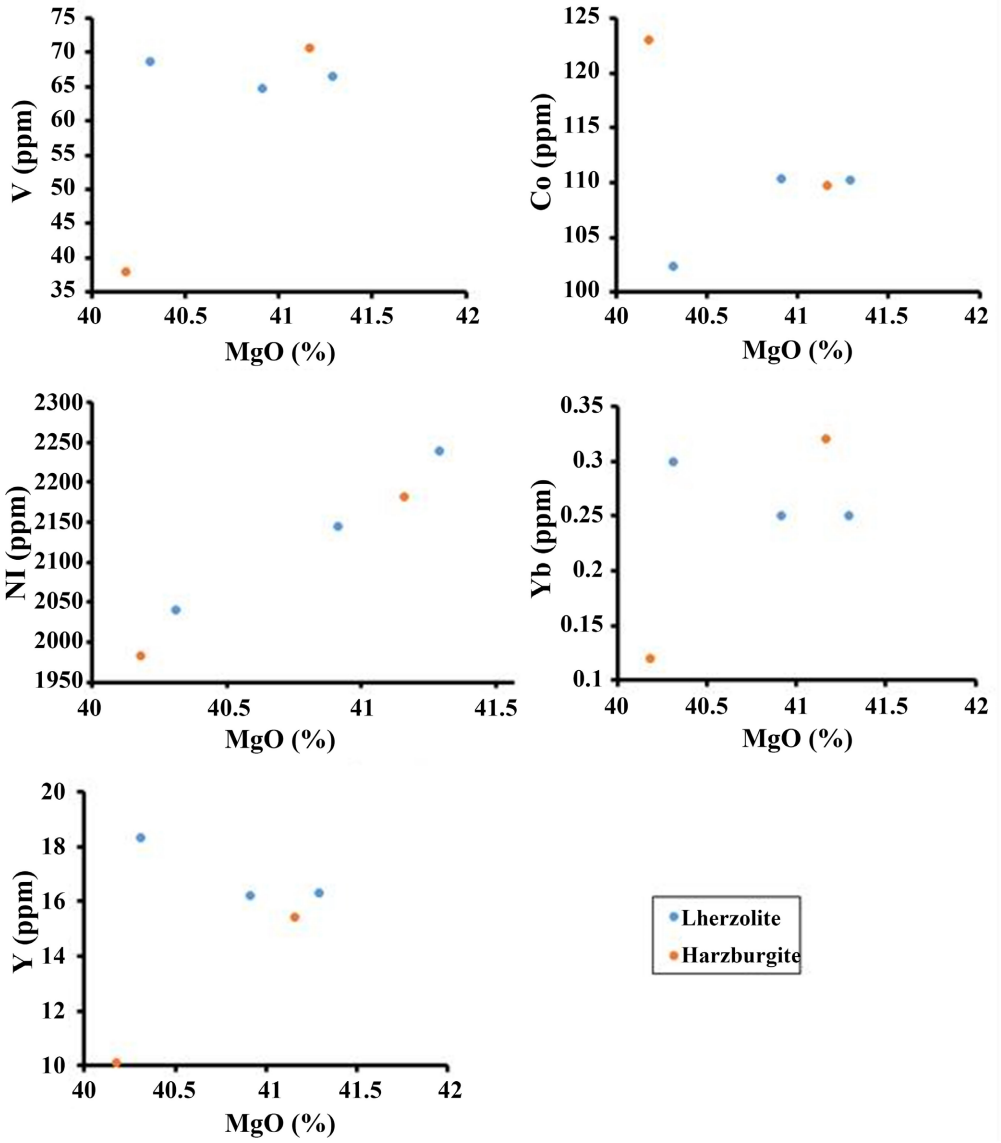

Figure 5. Variations of trace element (V, Co, Ni, Yb and Y) as a function of MgO.

type (i) samples or samples which display LREE depletion compare to MREE and less depleted HREE (see below).

Ti-Cr diagram of olivines (**Figure 7**) and NiO-Fo diagram of Cpx (**Figure 8**) reflect a particular position of wehrlite (far from the general trend) which the origin may be specified (see below).

Analysed lherzolites and harzburgites (five samples) are depleted in REE compare to the estimated primitive mantle values [30] except harzburgite NK04 which concentrations vary up to 5% of chondrites. In general, 2 types of REE patterns (**Figure 9**) are identified:

1) group 1 samples (lherzolites and harzburgites NK10) have "spoon shape" REE patterns (**Figure 9(A)**) and display LREE depletion compare to MREE and less depleted HREE; ($[La/Sm]_N$: 1.37 - 2.53; $[Sm/Yb]_N$: 0.33 - 0.47 et $[La/Yb]_N$: 0.46 - 1.28). A slight La-Ce "inflexions" is observed. Their multi-element REE

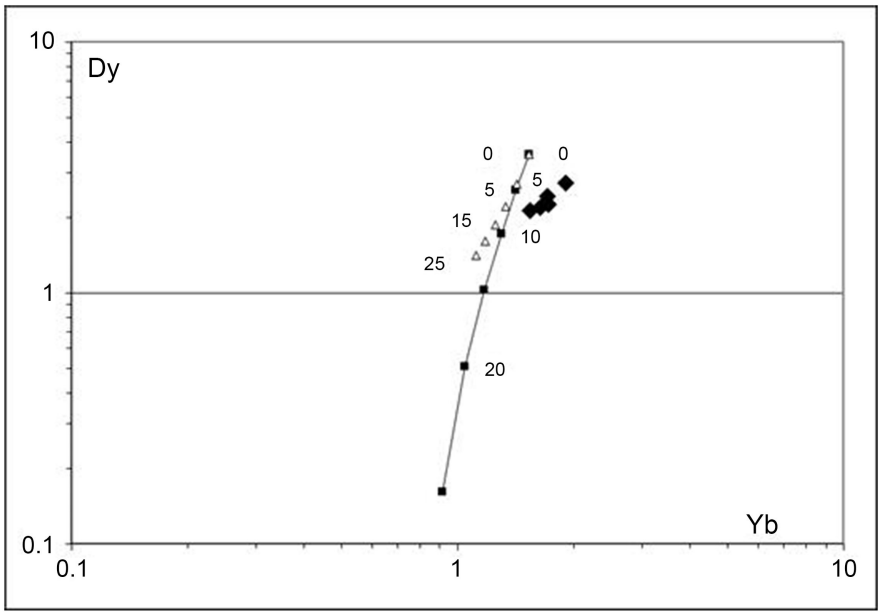

Figure 6. Dy vs Yb diagram of the clinopyroxene type (i) of Nyos ("spoon shape patterns"). Samples (diamond-shaped) project near the theorical curves of partial melting (black squares: fractional melting and white triangles: batch melting). Modelisation after Johnson *et al.* [28]. Values of the initial composition of primary peridotite were taken after Sun and McDonough [29] and McDonough and Sun [30]. Note that Nyos peridotites of type (i) project near partial melting curves, and gather together for degree of partial melting mostly around 5%.

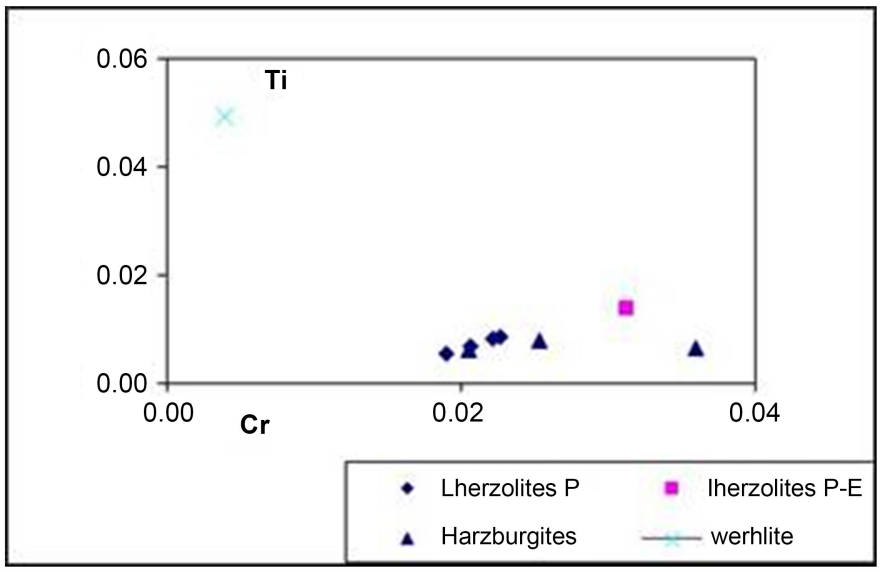

Figure 7. Ti-Cr Diagram of the olivines from Nyos peridotites (mean compositions per sample). P: porphyroclastic texture, P-E: porphyroclastic to equigranular texture.

patterns (**Figure 9(B)**) are similar and characterize by negative anomalies in Rb and Sr.

2) REE patterns of harzburgite rich phlogopite NK04 (**Figure 9(A)**) are characterized by a "convex" shape enriched in LREE compare to MREE and HREE;

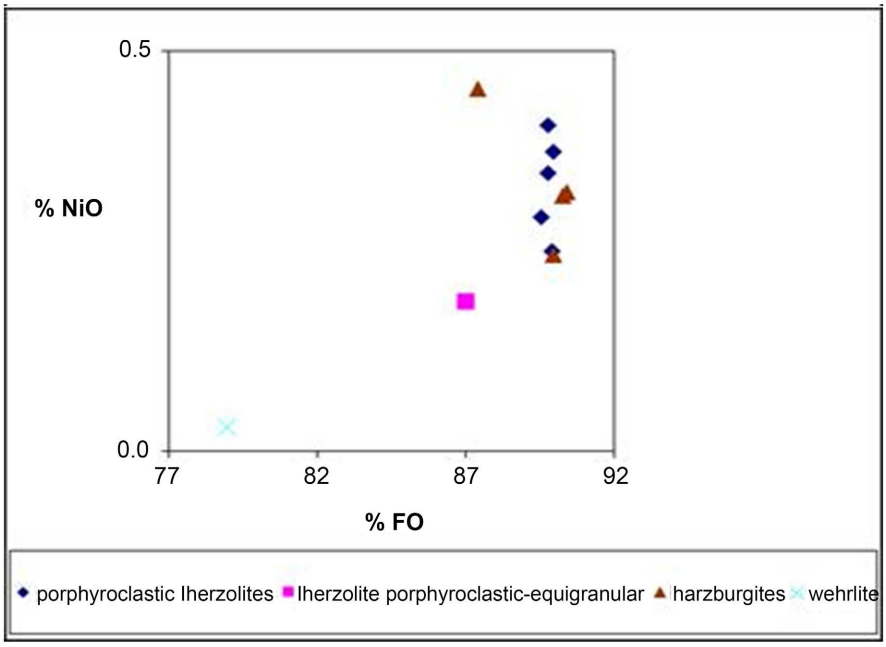

Figure 8. NiO-Fo Diagramm of the olivines from Nyos peridotites. (mean compositions per sample).

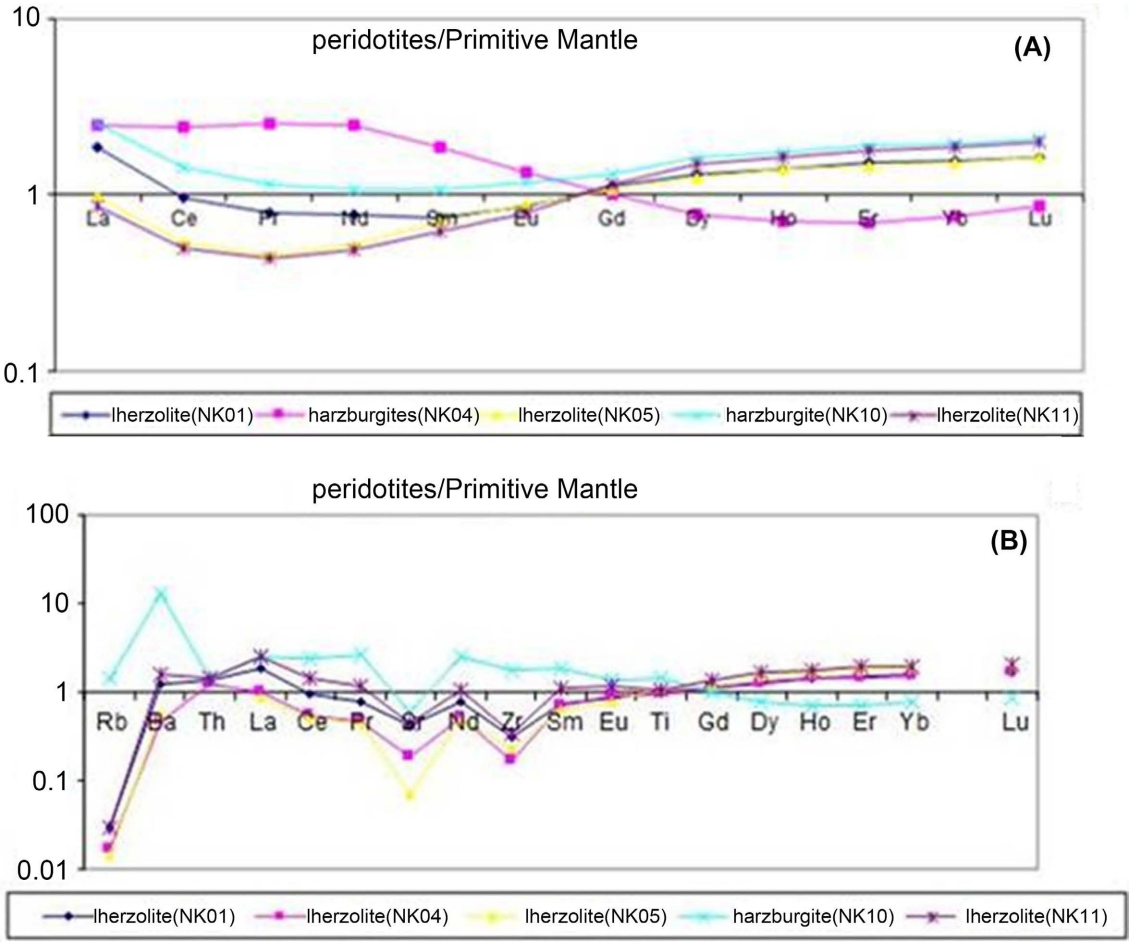

Figure 9. Bulk rock REE (A) and multi-element (B) patterns of Nyos peridotites.

$[La/Sm]_N$: 0.43 - 1.34; $[Sm/Yb]_N$: 0.33 - 0.55 et $[La/Yb]_N$: 0.46 - 1.28). Multi-element REE patterns (**Figure 9(b)**) of harzburgite NK04 point out a deep negative anomalies of Rb and positive anomalies in Sr.

LREE enrichments in some samples compare to MREE, positive anomalies in Sr as well as the crystallization of mantle amphiboles and phlogopites, are generally considered to be a result of interactions between melts or fluids and the surrounding mantle rocks (e.g., O'Reilly and Griffin, [31]; Coltorti *et al.* [32]; Van Achterbergh *et al.* [33]; Grégoire *et al.* [34] [35]). Thus, it appears that the studied mantle xenoliths from Nyos record metasomatic processes.

4. Thermometric Data

Several experimental and theoretical attempts have been made to investigate the temperature dependence of Mg-partitioning between ortho and clinopyroxene in order to evaluate the equilibrium temperatures for natural assemblages. The same process of temperature evaluation can be investigate between olivine and spinel as most samples rich in spinel show no or less zoning and generally display porphyroclastic to equigranular texture: an argument to estimate the evolution of the re-equilibrium temperature in the same mineral or a couple of minerals. Three geothermometers have been used in the present work [36] [37] [38] and results are shown in **Table 5**.

5. Discussion

Evidence from ultramafic xenoliths suggests that the upper mantle sampled by alkali basalts of the LNVU is predominantly composed of spinel lherzolites and

Table 5. Equilibrium temperatures of peridotites from Lake Nyos Volcanic Unit, based on various thermometers.

Samples sample	T(F)	T(W)	T(BK)
NK01 (LP)	770	938	973
NK05 (LP)	790	952	955
NK07 (LP)	788	968	986
NK09 (LP)	-	933	971
NK11 (LP)	787	944	990
NK14 (LP-E)	901	1000	1040
NK02 (H)	883	962	994
NK04 (H)	796	904	907
NK10 a (H)	816	978	1025
NK10 b (H)	775	940	966

T(W) = Thermometer of Wells [37] Opx-Cpx association; T(F) = Thermometer of Fabries [36], Ol-Sp association; T(BK) = Thermometer of Brey and Koeler [38], respectively solvus, Na-pyroxenes and Fe-Mg; LP: Lherzolite with Porphyroclastic texture; LP-E: Lherzolite transitional Porphyroclastic to Equigranular texture; H: Harzburgite.

spinel harzburgites. Nonetheless, a closer examination of these xenoliths clearly shows that the upper mantle is highly inhomogeneous with respect to the texture as well as major and trace element geochemistry. The systematic trends observed in the xenoliths and their constituent minerals are discussed in terms of partial melting and metasomatism (for more details, see; Teitchou *et al.* [10] and figures therein). The depletion of some elements such as Al, Ti, Ca, Y and HREE in bulk rocks, together with the increase of both Mg-number and Ni in olivine and Cr/Al ratio in spinel from lherzolites I to harzburgites are well expression of the depleted material. Group 2 xenoliths are relatively Fe-rich, which is not typical for normal lithospheric mantle. Fe-rich mantle here is probably related to circulation within the depleted mantle of a large volume of these more or less alkaline and carbonate-rich mafic silica melts [10]. Comparison of our data with those of Lee *et al.* [39] shows that, except for Sc, the abundance of the compatible trace elements is closely similar.

Metasomatism results from the transfer from the asthenosphere to the lithosphere of alkaline magmatic liquids rich in volatiles and changes in the Temperature and fugacity in Oxygen (T-fO_2) mantle array, confirm by the fact that CO_2-rich inclusions occur exclusively in clinopyroxenes [19]. Thus CO_2 formation is a consequence of mantle metasomatism [19].

This transfer would trigger intense modal (appearance of amphiboles and phylogopites) and cryptic metsomatism (REE enrichments) of the upper mantle and explosive volcanism. The contamination of lithospheric peridotites by these liquids coming from the asthenosphere accounts for the presence of pargasite in the hydrated samples (rich in H_2O) and the wide dispersion of certain elements such as REE. Ti rich, Cr poor and low values of NiO and F_O (%) in wehrlite compare to other xenoliths (**Figure 7** and **Figure 8**) are also indicating of metasomatism. The low Fo values of olivines can be impute to the re-equilibration between olivine and a liquid rich in Fe [40] or to mantle metasomatism generated by basaltic magma infiltrations ("Fe-Ti metasomatism", [41] [42]). These low values also suggest that after their formation, wehrlite were percolated by, and re-equilibrated within basaltic magmas outled by low degrees of partial melting estimate above of around 5%. The metasomatic liquid which percolated the lithospheric column was a densely silicate rich in volatile and able to transport a high quantity of Ti. Metasomatic events due to percolation through peridotites of a liquid rich in H_2O, Ti, Fe, Na and K (Fe-Ti metasomatism) is mineralogically recorded by pargasitic amphiboles.

In detail, the examination of highly metasomatised rocks (samples NK02, NK04, NK08, NK14) point out the fact that:

1) clinopyroxene REE patterns of those rocks are convex, enriched in LREE and MREE compare to HREE with an exception for harzburgites bearing amphibole NK02 characterize by a constant MREE and HREE. Nevertheless, they display same negative anomalies in HFSE (Ti, Nb, Ta) and positive anomalies in Th, U, La and Sr (**Figure 10(A)**).

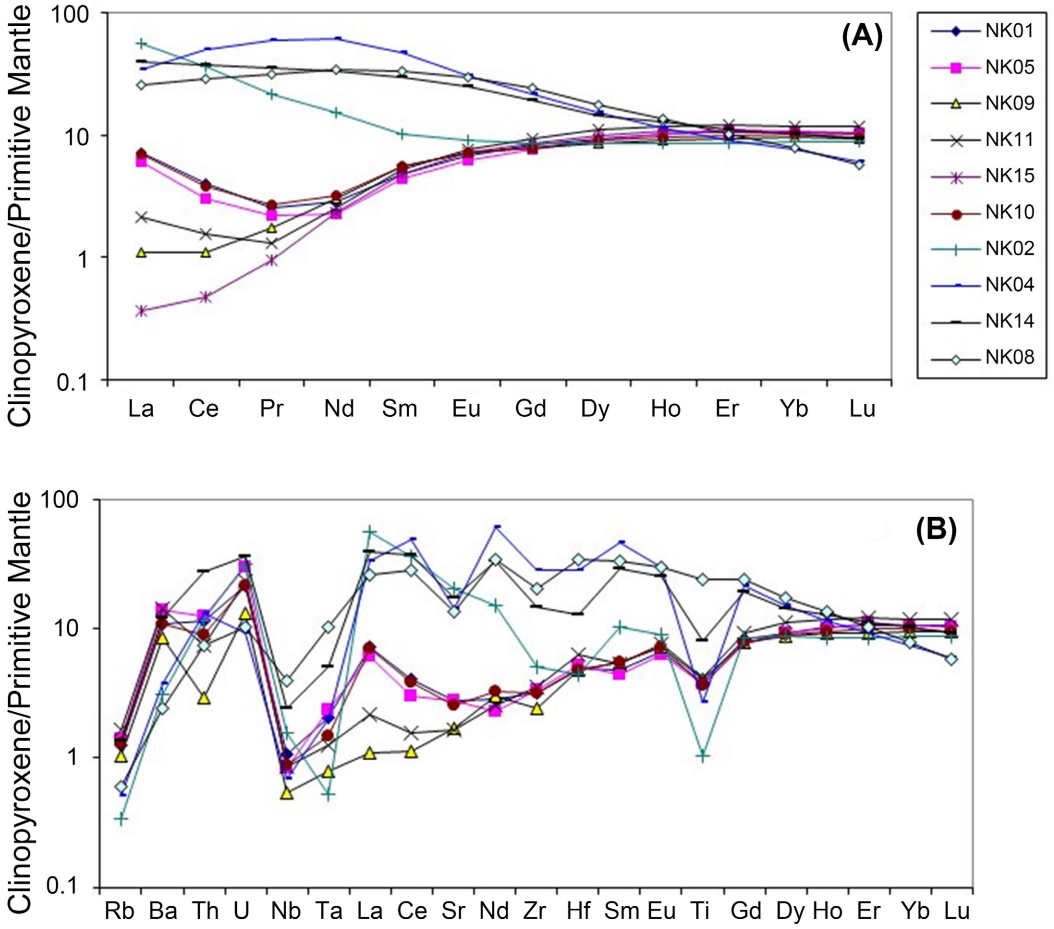

Figure 10. REE (A) and multi element (B) patterns of CPX of Nyos peridotites (normalization values after); McDonough and Sun [30].

2) overall or multi-element clinopyroxene trace elements of hydrous samples (NK02, NK04) and lherzolite NK14 are characterize by negative anomalies in HFSE (Nb, Ta, Zr, Hf and Ti) and positive anomalies in Rb, Th and U (**Figure 10(B)**).

3) multi-element clinopyroxene trace element patterns of anhydrous samples (NK08 and NK14, **Figure 10(B)**) are similar and display positive anomalies in U, La, Zr and negative anomalies in HFSE (Nb, Sr, Ti).

These observations are consistent with the fact that:

- clinopyroxenes are the main hosts of trace elements during partial melting of Nyos peridotites,
- the HFSE depletion trends appear to reflect low HFSE abundances in the metasomatic hydrous melts compared to the LILE, consequently, the flux of HFSE through the mantle wedge was low, corroborate by high LREE/HFSE and LILE/HFSE ratios,
- anhydrous metasomatised peridotites experience enrichments only in HFSE melts while hydrous metasomatised peridotites experienced both enrichment in HFSE and alkali melts,
- clinopyroxenes, amphiboles and phlogopites are good reservoirs of HFSE of

the studied peridotites while REE budget is shared by amphiboles and clinopyroxenes, confirm by their parallel REE patterns enriched in LREE compared to constant MREE and HREE, and also by their strong positive anomalies in Sc, Th and La and negative anomalies in Ti and Ta [10] (see **Figure 5** therein).

Ultramafic xenoliths from LNVU are similar in their major and minor element mineral and bulk rock chemistry to numerous other xenoliths from the continental and oceanic part of the CVL [4] [12] [15] and elsewhere (e.g. Spitsbergen, Ionov *et al.* [25]).

The temperatures obtained (**Table 5**) on Nyos peridotites vary between 770˚C and 1040˚C. Sample NK14 exhibits higher temperature (1040˚C) compare to other xenoliths, it shows aggregates of spinels and pyroxenes, resulting of the destabilization of old garnet [15] [22] [43] amongst others.

Pyroxenic geotherms suggest that the majority of peridotite xenoliths were equilibrated between 900˚C and 1000˚C under spinel upper mantle conditions. As a result, this study makes it possible to propose two distinct stages in the history of Nyos peridotites:

- Temperatures above 1000˚C testify the fact that some peridotites could have been equilibrated in the garnet stability domain before undergoing a diapiric uplift and requilibrated into the spinel facies. The upper parts of the ascending diapirs would have been laminated as evidenced by the texture of the NK14 sample (transitional porphyroclastic to equigranular, **Figure 3(C)**). These results would thus confirm the existence of asthenospheric diapirs directly below the upper mantle of Nyos as suggested by Teitchou *et al.* [44]:
- Temperatures between 900˚C and 1000˚C correspond to the prevailing conditions before the mantle rose prior the eruption that brought these peridotites to the surface.

It should be noted that the temperatures obtained from the Fabries thermometer (770˚C - 901˚C) are lower than those described above, probably because of the diapiric rises (gradual drop in temperature and especially because the spinel crystals are altered in surface conditions, alteration figures were observed during the microscopic study). This thermometer from Fabries [36], in our case (spinel peridotites) thus gives more credibility to the above interpretations and probably corresponds to the temperature before the starting of the eruption. It is known that there are no reliable geobarometers applicable for the Nyos assemblage types (spinel peridotites). Nonetheless the gravity and seismic data of the crust under the CVL show a normal thickness of about 30 km at the Nyos volcano, corresponding to pressures of 8 Kbar if we consider an average crust density of 2.7 [45] and an estimation of the lithosphere-asthenosphere boundary at about 90 km [46]. In addition, the report of the temperatures obtained in this work in the P-T diagram of Mercier and Carter [47] applicable for rifting context, we estimate the pressures from 8 to 18 Kbar corresponding to depths of 50 to 30 km (**Figure 11** and see text for explanation), pressures in which studied xenoliths were incorporated in the host lavas, except sample NK14.

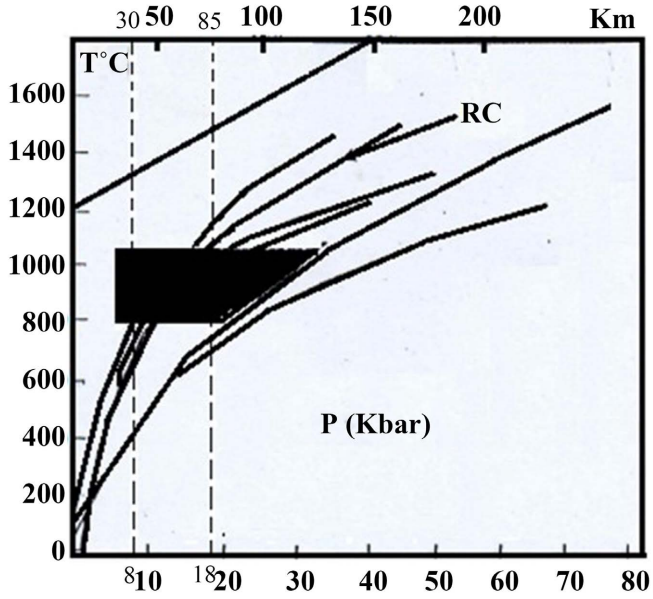

Figure 11. Position of the Nyos xenoliths in the P-T stability diagram of mantle peridotites, according to the rift-type geotherm [48]. The curves correspond to the different possible experimental evolutions depending on the depth. For the case of Nyos, the possible evolution is that indicated by the reference curve (RC) corresponding to 8 Kbar and cutting the temperature field at depths between 85 and 30 km.

Aka [48] indicates that the depth of melt segregation below the Nyos maar-diatreme volcano is shallower. The supposed shallow depth of the asthenophere beneath the LNVU indicates that the deepest xenoliths brought up by the basaltic eruption originate from a mantle region not much shallower than the source regions of basaltic magma. The lack of garnet lherzolithic xenoliths here and in most alkali basaltic rock associated with continental rift zones is an argument in favor of relatively shallower position of the magmatic source, but our investigations show that the magma source, which generated the volcanism at LNVU, lies probably in the deepest part of the upper mantle, near the top of the garnet peridotite field, confirm by sample NK14 displaying old garnet signature. The mechanism of this transfer from deeper to shallower depths is similar to that of polydiapirs, also developed for the French Massif Central [49].

Field evidence from lherzolite massifs related to asthenosphere upwelling [15] [18], tomographic studies [9] [46] [50] and recent survey reports of the NMDP (Nyos Monoun Degassing Project) suggest that the upwelling occurred within a narrow and steep conduits, implying a lithospheric rupture, which create, in the upper crust, narrow troughs, with expansion being mainly caused by intrusion of mantle wedges at depth and expansion of basalt flows and basalt dykes described by Aka *et al.* [14]. Metasomatism of carbonatitic affinity caused overall oxidation of the upper mantle which is at origin of continuous accumulation of huge quantity of CO_2 under the lake through some conduits or special weak points which can be released in the surface (like the lethal gas, killing 1746 human being and plenty animals, like the 1986 catastrophe) probably by the me-

chanism of double density inversion between H_2O and CO_2 proposed by Touret *et al.* [19].

The thermomechanical conditions described above and the behaviour of a stable continental lithosphere subjected to stretching suggests that the lithosphere has been previously weakened (rift zone initiators?). Therefore, the presence of rising mantle plume is probably related to the evolution of heteregenous translithospheric mantle diapirs beneath this section of the continental CVL. Local diapirs here may be interpreted as direct or indirect rift-zone initiators. The term of this mantle wedges uplifting, if they were to continue, would be a thinning of the crust, followed by the rupture and the creation of a rift. Therefore, the CVL can be considered as an aborted rift.

6. Conclusions and Point of View

The examination of petrological and geochemical features of the studied peridotite xenoliths provided insight into the upper mantle below the Lake Nyos and revealed the existence of chemical inhomogeneities that seem to be related to two different processes. The first one was connected with the equilibrium partial melting event that produced a continuous series of peridotites from undepleted to deplete. The second one concerns xenoliths designated as metasomatized. Metasomatism, which can be cryptic or modal, caused overall oxidation of the upper mantle beneath this area and CO_2 abnormal concentration beneath the Lake. Geochemical data indicate that the Nyos mantle column were percolated by a dense alkaline silicate rich in volatile, displaying low HFSE abundances in the metasomatic hydrous melts compared to the LILE.

The xenoliths were initially equilibrated in the garnet stability field, at depth of 85 km. Then, they were "re-equilibrated" in the spinel field owing to isobaric heating up to 900˚C - 1000˚C. Textural evidence and P-T estimated show that the mantle is moderately tectonized and associated xenoliths display a large range of depths from the crust-mantle boundary (30 Km) to the deeper garnet facies (>85 Km), materialized here by sample NK14 showing transitional porphyroclast to equigranular texture and displaying pyroxene-Cr spinel symplectites. It is suggested that the observed ultramafic suite were first sampled by basaltic magmas at the lower lithosphere, then were percolated and eroded by plume-derived basaltic melts from 8 to 18 Kbar corresponding to pressure in which most xenoliths were incorporated in the host lavas at depths of 50 to 30 Km before their transit to the surface.

The thermomechanical setting was favorable to asthenosphere upwelling which generates lithospheric rupture on narrow troughs (probably expand to form local diapirs), and consequently, intrusion of mantle wedges occurs at depth and expansion of basalt following the rifting model.

This study comforts the idea that Cameroon Volcanic Line represents several independent translithospheric mantle diapirs. Thus, giving partial answers to the question of why some volcanic lakes with similar eruptive style like Lake Nyos

do not contain a huge quantity of CO_2 at their bottom? High temperatures were obtained in some samples, and different textures (deformations and recrystallization) observed as well as the mantle metasomatism would be, in our opinion, the results of the asthenospheric uplift during the Pan-African event and the opening of the Central Atlantic Sea.

Acknowledgements

This work was funded by a French Government Scholarship and supported by the Institute of Geological and Mining Research, IRGM-Cameroon. Dr. Diouta G and Kamani Toko of ISTIC Bangangte are appreciated for their support.

Conflicts of Interest

The authors declare no conflicts of interest regarding the publication of this paper.

References

[1] Moreau, C., Regnoult, T.M., Déruelle, B. and Robineau, B. (1987) A New Tectonic Model for Cameroon Line, Central Africa. *Tectonophysics*, **139**, 317-334. https://doi.org/10.1016/0040-1951(87)90206-X

[2] Déruelle, B., Moreau, C., Nkoumbou, C., Kambou, R., Lissom, J., Njonfang, E., Ghogomu, R.T. and Nono, A. (1991) The Cameroon Line: A Review. In: Kampunzu, A.B. and Lubala, R.T., Eds., *Magmatism in Extensional Structure Setting*, Springer-Verlag, Heidelberg, 274-328. https://doi.org/10.1007/978-3-642-73966-8_12

[3] Déruelle, B., Ngounouno, I. and Demaiffe, D. (2007) The "Cameroon Hot Line" (CHL): A Unique Example of Active Alkaline Intraplate Structure in both Oceanic and Continental Lithospheres. *Comptes Rendus Geoscience*, **339**, 589-600. https://doi.org/10.1016/j.crte.2007.07.007

[4] Lee, D.C., Halliday, A.N., Fitton, G. and Poli, G. (1994) Isotopic Variations with Distance and Time in the Volcanic Islands of the Cameroon Line—Evidence for a Mantle Plume Origin. *Earth and Planetary Science Letters*, **123**, 119-138. https://doi.org/10.1016/0012-821X(94)90262-3

[5] Meyers, J.B., Rosendahl, B.R., Harrison, C.G.A. and Zan-Dong, D. (1998) Deep-Imaging Seismic and Gravity Results from the Offshore Cameroon Volcanic Line, and Speculation of African Hotlines. *Tectonophysics*, **284**, 31-63. https://doi.org/10.1016/S0040-1951(97)00173-X

[6] Fitton, J.C. (1987). The Cameroon Line—West Africa: A Comparison between Oceanic and Continental Alkaline Volcanism. *Geological Society Special Publications*, **30**, 273-291. https://doi.org/10.1144/GSL.SP.1987.030.01.13

[7] Halliday, A.N., Dickin, A.P., Fallick, A.F. and Fitton, J.G. (1988) Mantle Dynamics: A Nd, Sr, Pb and O Study of the Cameroon Line Volcanic Chain. *Journal of Petrology*, **29**, 181-211. https://doi.org/10.1093/petrology/29.1.181

[8] Montigny, R., Ngounouno, I. and Déruelle, B. (2004) Ages K-Ar des roches magmatiques du fossé de Garoua (Cameroun): Leur place dans le cadre de la "Ligne du Cameroun". *Comptes Rendus Geoscience*, **336**, 1463-1471. https://doi.org/10.1016/j.crte.2004.08.005

[9] Reusch, A.M, Nyblade, A.A., Wiens, D.A., Shore, J.P., Ateba, B., Tabod, C.T. and

Nnange, J.M. (2010) Upper Mantle Structure beneath Cameroon from Body Wave Tomography and the Origin of the Cameroon Volcanic Line. *Geochemistry Geophysics Geosystems*, **11**, Q10W07. https://doi.org/10.1029/2010GC003200

[10] Teitchou, M.I., Grégoire, M., Temdjim, R., Ghogomu, R.T., Ngwa, C. and Aka, F.T. (2011) Mineralogical and Geochemical Fingerprints of Mantle Metasomatism beneath Nyos Volcano (Cameroon Volcanic Line). In Beccaluva, L., Bianchini, G. and Wilson, M., Eds., *Volcanism and Evolution of the African Lithosphere*, Geological Society of America Special Paper, 478, Boulder, 193-210. https://doi.org/10.1130/2011.2478(10)

[11] Njome, M.S. and De Wit, M.J. (2014) The Cameroon Line: Analysis of an Intraplate Magmatic Province Transecting both Oceanic and Continental Lithospheres: Constraints, Controversies and Models. *Earth-Science Reviews*, **139**, 168-194. https://doi.org/10.1016/j.earscirev.2014.09.003

[12] Nana, R. (2001) Pétrologie des péridotites en enclaves dans les basaltes alcalins récents de Nyos: Apport à la connaissance du manteau supérieur de la Ligne du Cameroun. Thèse doctorat d'Etat Universite de Yaoundé I, Yaoundé, 250 p.

[13] Aka, F.T., Nagao, K., Kusakabe, M. and Ntepe, N. (2009) Cosmogenic Helium and Neon in Ultramafic Xenoliths from the Cameroon Volcanic Line (West Africa): Preliminary Observations. *Journal of African Earth Sciences*, **55**, 175-184. https://doi.org/10.1016/j.jafrearsci.2009.04.002

[14] Aka, F.T., Hasegawa, T., Nche, L.A., Asobo, N.E.A., Mimba, M.E., Teitchou, I., Ngwa, C.N., Miyabuchi, Y., Kobayashi, T., Kankeu, B., Yokoyama, T., Tanyileke, G., Ohba, T., Hell, J.V. and Kusakabe, M. (2018) Upper Triassic Mafic Dykes of Lake Nyos, Cameroon (West Africa) I: K-Ar Age Evidence within the Context of Cameroon Line Magmatism, and the Tectonic Significance. *Journal of African Earth Sciences*, **141**, 49-59. https://doi.org/10.1016/j.jafrearsci.2018.02.001

[15] Teitchou, M.I., (2008) Volcanologie, pétrologie et géochimie comparées de quelques plaines continentales (Kumba, Tombel, Noun, Nyos) de la Ligne du Cameroun. PHD Thesis, University of Yaoundé I, Yaoundé, 206 p.

[16] Streckeisen, A. (1976) To Each Plutonic Rock Its Proper Name. *Earth-Science Reviews*, **12**, 1-33. https://doi.org/10.1016/0012-8252(76)90052-0

[17] Temdjim, R., Boivin, P., Chazot, G., Robin, C. and Rouleau, E. (2004) L'hétérogénéité du manteau supérieur à l'aplomb du volcan de Nyos (Cameroun) révélée par les enclaves ultrabasiques. *Comptes Rendus Geoscience*, **336**, 1239-1244. https://doi.org/10.1016/j.crte.2004.07.005

[18] Temdjim, R. (2012) Ultramafc Xenoliths from Lake Nyos Area, Cameroon Volcanic Line, West-Central Africa: Petrography, Mineral Chemistry, Equilibration Conditions and Metasomatic Features. *Chemie der Erde*, **72**, 39-60. https://doi.org/10.1016/j.chemer.2011.07.002

[19] Touret, J., Grégoire, M. and Teitchou, M.I. (2010) Was the Letal Eruptrion of Lake Nyos Relted to Double CO_2/H_2O Density Inversion? *Comptes Rendus Geoscience*, **341**, 19-26. https://doi.org/10.1016/j.crte.2009.10.005

[20] Leake, B.E. (1978) Nomenclatures of Amphiboles. *The American Mineralogist*, **63**, 1023-1052.

[21] Frey, F.A. and Prinz, M. (1978) Ultramafic Inclusions from San Carlos (Arizona), Petrologic and Geochemical Data Bearing of Their Petrogenesis. *Earth and Planetary Science Letters*, **38**, 139-176. https://doi.org/10.1016/0012-821X(78)90130-9

[22] Lenoir, X., Garrido, C.J., Bodinier, J.-L. and Dautria, J.-M. (2000) Contrasting Lithospheric Mantle Domains beneath the Massif Central (France) Revealed by Geo-

chemistry of Peridotite Xenoliths. *Earth and Planetary Science Letters*, **181**, 359-375. https://doi.org/10.1016/S0012-821X(00)00216-8

[23] Lenoir, X., Garrido, C.J., Bodinier, J.-L., Dautria, J.-M. and Gervilla, F. (2001) The Recrystallization Front of the Ronda Peridotite: Evidence for Melting and Thermal Erosion of Subcontinental Lithospheric Mantle beneath the Alboran Basin. *Journal of Petrology*, **42**, 141-158. https://doi.org/10.1093/petrology/42.1.141

[24] Jagoutz, E., Palme, H., Baddenhauser, H., Blum, K., Cendales, M., Dreibus, G., Spettel, B., Lorenz, V. and Wänke, H., (1979) The Abundance of Major, Minor and Trace Elements in the Earth's as Derived from Primitive Ultramafic Nodules. *Lunar and Planetary Science Conference X*, Houston, 19-23 March 1979, 2031-2050.

[25] Ionov, D.A., Bodinier, J.-L., Mukasa, S.B. and Zanetti, A., (2002) Mechanism and Sources of Mantle Metasomatism: Major and Trace Element Compositions of Peridotites Xenoliths from Spitsbergen in the Context of Numerical Modelling. *Journal of Petrology*, **43**, 2219-2259. https://doi.org/10.1093/petrology/43.12.2219

[26] Grégoire, M., Lorand, J.P., Cottin, J.Y., Giret, A., Mattielli, N. and Weiss, D. (1997) Xenoliths Evidence for a Refractory Oceanic Mantle Percolated by Basaltic Melts beneath the Kerguelen Archipelago**.** *European Journal of Mineralogy*, **9**, 1085-1100. https://doi.org/10.1127/ejm/9/5/1085

[27] Bjerg, E.A., Ntaflos, T., Kurat, G., Dobosi, G. and Labudia, C.H. (2005) The Upper Mantle beneath Patagonia, Argentina, Documented by Xenoliths from Alkali Basalts. *Journal of South American Earth sciences*, **18**, 125-145. https://doi.org/10.1016/j.jsames.2004.09.002

[28] Johnson, K.T.M., Dick, H.J.B. and Shimizu, N. (1990) Melting in the Oceanic Mantle: An Ion Microprobe Study of Diopsides in Abyssal Peridotites. *Journal of Geophysical Research*, **95**, 2661-2678. https://doi.org/10.1029/JB095iB03p02661

[29] Sun, S.S. and McDonough, W.F. (1989) Chemical and Isotopic Systematics of Oceanic Basalts: Implications for the Mantle Composition and Processes. In: Saunders, A.D. and Norry, M.J., Eds., *Magmatism in the Oceanic Basin*, Blackwell Scientific Publications, Oxford, 313-346. https://doi.org/10.1144/GSL.SP.1989.042.01.19

[30] McDonough, W.F. and Sun, S.-S. (1995) The Composition of the Earth. *Chemical Geology*, **20**, 223-253. https://doi.org/10.1016/0009-2541(94)00140-4

[31] O'Reilly, S.Y. and Griffin W.L. (2010) The Continental Lithosphere-Asthenosphere Boundary: Can We Sample It? *Lithos*, **120**, 1-13. https://doi.org/10.1016/j.lithos.2010.03.016

[32] Colcorti, M., Bonadiman, C., Hinton, R.W., Siena, F. and Upton, B.G.J. (1999) Carbonatite Metasomatism of the Oceanic Upper Mantle: Evidence from Clinopyroxenes and Glasses in Ultramafic Xenoliths of Grande Comores, Indian Ocean. *Journal of Petrology*, **40**, 135-165. https://doi.org/10.1093/petroj/40.1.133

[33] Van Achterbergh, E., Griffin, W.L. and Stiefenhofer, J. (2001) Metasomatism in Mantle Xenoliths from the Letlhakane Kimberlites: Estimation of Element Fluxes. *Contributions to Mineralogy and Petrology*, **141**, 397-414. https://doi.org/10.1007/s004100000236

[34] Grégoire, M., Bell, D.R. and Le Roex, A.P. (2003) Garnet Lherzolites from the Kaapvaal Craton South Africa: Trace Element Evidence for a Meta-Somatic History. *Journal of Petrology*, **44**, 629-657. https://doi.org/10.1093/petrology/44.4.629

[35] Grégoire, M., Tinguely, C., Bell, D.R. and Le Roex, A.P. (2005) Spinel Lherzo-Lite Xenoliths from the Premier Kimberlite (Kaapvaal Craton, South Africa): Nature and Evolution of the Shallow Upper Mantle beneath the Bushveld Complex. *Lithos*,

84, 185-205. https://doi.org/10.1016/j.lithos.2005.02.004

[36] Fabriès, J. (1987) Spinel-Olivine Geothermobarometry in Peridotites from Ultramafic Complexes. *Contributions to Mineralogy and Petrology*, **69**, 329-336. https://doi.org/10.1007/BF00372258

[37] Wells, P.R.A. (1977) Pyroxene Thermometry in Simple and Complex System. *Contributions to Mineralogy and Petrology*, **62**, 129-139. https://doi.org/10.1007/BF00372872

[38] Brey, G.P. and Köhler, T. (1990) Geothermobarometry in Four-Phase Lherzo-Lites II. New Thermobarometers and Practical Assessment of Existing Thermobarometers. *Journal of Petrology*, **31**, 1353-1378. https://doi.org/10.1093/petrology/31.6.1353

[39] Lee, D.C., Halliday, A.N, Gareth, R.D, Essene, E.J, Fitton, J.G. and Temdjim, R. (1996) Melt Enrichment at Shallow Depleted Mantle: A Detail Petrological, Trace Element and Isotopic Study of Mantle Derived Xenoliths and Megacrysts from the Cameroon Line. *Journal of Petrology*, **47**, 415-441. https://doi.org/10.1093/petrology/37.2.415

[40] Girardeau, J. and Francheteau, J. (1993) Plagioclase-Wehrlites and Peridotites on the East Pacific Ridge (Hess Dufi) and the Mid Atlantic Ridge (DSPP Sole, 33W): Evidence for Magma Percolation in the Oceanic Upper Mantle. *Earth and Planetary Science Letters*, **115**, 137-149. https://doi.org/10.1016/0012-821X(93)90218-X

[41] Menzies, M.A., Arculus, R.J., Best, M.G., Bergman, S.C., Ehrenberg, S.N., Irving, A.J., Roden, M.F. and Schule, D.J. (1987) A Record of Subduction Processes and Within-Plate Volcanism of the Southern USA. In: Nixon, P.H., Ed., *Mantle Xenoliths*, John Wiley et Sons, Chichester, 41-58.

[42] Bodinier, J.-L., Vasseur, G., Vernières, J., Dupuy, C. and Fabriès J. (1990) Mechanism of Mantle Metasomatism: Geochemical Evidence from the Lherz Orogenic Peridotite. *Journal of Petrology*, **31**, 597-628. https://doi.org/10.1093/petrology/31.3.597

[43] Fabries, J., Lorand, J.-P., Bodinier, J.-L. and Dupuy, C. (1991) Evolution of the Upper Mantle beneath the Pyrenees: Evidence from Orogenic Spinel Lherzolite Massifs. *Journal of Petrology*, **2**, 55-76. https://doi.org/10.1093/petrology/Special_Volume.2.55

[44] Teitchou, M.I., Grégoire, M., Dantas, C., Tchoua, F.M. (2007) Le manteau supérieur à l'aplomb de la plaine de Kumba (ligne du Cameroun), d'après les enclaves de péridotites à spinelles dans les laves basaltiques. *Comptes Rendus Geoscience*, **339**, 101-109. https://doi.org/10.1016/j.crte.2006.12.006

[45] Poudjom Djomani, Y.H., Diament, M. and Wilson, M. (1997) Lithospheric Structure across the Adamawa Plateau (Cameroon) from Gravity Studies. *Tectonophysics*, **273**, 317-327. https://doi.org/10.1016/S0040-1951(96)00280-6

[46] Fishwick, S. (2010) Surface Wave Tomography: Imaging of the Lithosphere-Asthenosphere Boundary beneath Central and Southern Africa? *Lithos*, **120**, 63-73. https://doi.org/10.1016/j.lithos.2010.05.011

[47] Mercier, J.C. and Carter, L.N. (1977) Pyroxene Geotherms. *Journal of Geophysical Research*, **80**, 3349-3362. https://doi.org/10.1029/JB080i023p03349

[48] Aka, F.T. (2015) Depth of Melt Segregation below the Nyos Maar-Diatreme Volcano (Cameroon, West Africa): Major-Trace Element Evidence and Their Bearing on the Origin of CO_2 in Lake Nyos. In: *Volcanic Lakes*, Springer, Berlin, 467-488. https://doi.org/10.1007/978-3-642-36833-2_21

[49] Boivin, P. (1982) Interactions entre magmas basaltiques et manteau supérieur.

Arguments apportés par les enclaves basiques des basaltes alcalins. Exemples de Devès (Massif Central Français) et du volcanisme quaternaire Carthagène (Espagne). Thèse d'état, Université de Clermont II, Clermont, 344 p.

[50] Goussi Ngalamo, J.F., Sob, M., Bisso, D., Abdelsalam, M.G., Atekwana, E. and Ekodeck, G.E. (2018). Lithospheric Structure beneath the Central Africa Orogenic Belt in Cameroon from the Analysis of satellite Gravity and Passive Seismic Data. *Tectonophysics*, **745**, 326-337. https://doi.org/10.1016/j.tecto.2018.08.015